POPDC1^{S201F} causes muscular dystrophy and arrhythmia by affecting protein trafficking

Roland F.R. Schindler,[1] Chiara Scotton,[2] Jianguo Zhang,[3] Chiara Passarelli,[2,4] Beatriz Ortiz-Bonnin,[5] Subreena Simrick,[1] Thorsten Schwerte,[6] Kar-Lai Poon,[1] Mingyan Fang,[3,7] Susanne Rinné,[5] Alexander Froese,[8] Viacheslav O. Nikolaev,[8,9] Christiane Grunert,[1] Thomas Müller,[10] Giorgio Tasca,[4] Padmini Sarathchandra,[1] Fabrizio Drago,[4] Bruno Dallapiccola,[4] Claudio Rapezzi,[11] Eloisa Arbustini,[12] Francesca Romana Di Raimo,[2] Marcella Neri,[2] Rita Selvatici,[2] Francesca Gualandi,[2] Fabiana Fattori,[4] Antonello Pietrangelo,[13] Wenyan Li,[3] Hui Jiang,[3] Xun Xu,[3] Enrico Bertini,[4] Niels Decher,[5] Jun Wang,[3,14,15] Thomas Brand,[1] and Alessandra Ferlini[2,16]

[1]Heart Science Centre, National Heart and Lung Institute, Imperial College London, Harefield, United Kingdom. [2]Unit of Medical Genetics, Department of Medical Sciences, University of Ferrara, Ferrara, Italy. [3]BGI-Shenzhen, Shenzhen, China. [4]IRCCS Ospedale Pediatrico Bambino Gesù, Rome, Italy. [5]Institute for Physiology and Pathophysiology, Vegetative Physiology, Philipps-University of Marburg, Marburg, Germany. [6]Institute of Zoology, University of Innsbruck, Innsbruck, Austria. [7]Division of Clinical Immunology, Department of Laboratory Medicine, Karolinska Institutet at Karolinska University Hospital Huddinge, Stockholm, Sweden. [8]Department of Cardiology and Pneumology, University of Göttingen, Göttingen, Germany. [9]Experimental Cardiovascular Research, University Medical Center, Hamburg, Germany. [10]Molecular Plant Physiology and Biophysics, University of Würzburg, Würzburg, Germany. [11]Cardiology, Department of Experimental Diagnostic and Specialty Medicine, Alma Mater Studiorum–University of Bologna, Bologna, Italy. [12]Center for Inherited Cardiovascular Diseases, IRCCS Foundation Policlinico San Matteo, Pavia, Italy. [13]Department of Internal Medicine, University of Modena, Modena, Italy. [14]Department of Biology, University of Copenhagen, Copenhagen, Denmark. [15]Princess Al Jawhara Center of Excellence in the Research of Hereditary Disorders, King Abdulaziz University, Jeddah, Saudi Arabia. [16]Dubowitz Neuromuscular Centre, Developmental Neuroscience Programme, University College of London, Institute of Child Health, London, United Kingdom.

The Popeye domain–containing 1 (*POPDC1*) gene encodes a plasma membrane–localized cAMP-binding protein that is abundantly expressed in striated muscle. In animal models, POPDC1 is an essential regulator of structure and function of cardiac and skeletal muscle; however, *POPDC1* mutations have not been associated with human cardiac and muscular diseases. Here, we have described a homozygous missense variant (c.602C>T, p.S201F) in POPDC1, identified by whole-exome sequencing, in a family of 4 with cardiac arrhythmia and limb-girdle muscular dystrophy (LGMD). This allele was absent in known databases and segregated with the pathological phenotype in this family. We did not find the allele in a further screen of 104 patients with a similar phenotype, suggesting this mutation to be family specific. Compared with WT protein, POPDC1^{S201F} displayed a 50% reduction in cAMP affinity, and in skeletal muscle from patients, both POPDC1^{S201F} and WT POPDC2 displayed impaired membrane trafficking. Forced expression of POPDC1^{S201F} in a murine cardiac muscle cell line (HL-1) increased hyperpolarization and upstroke velocity of the action potential. In zebrafish, expression of the homologous mutation (*popdc1*^{S191F}) caused heart and skeletal muscle phenotypes that resembled those observed in patients. Our study therefore identifies *POPDC1* as a disease gene causing a very rare autosomal recessive cardiac arrhythmia and LGMD, expanding the genetic causes of this heterogeneous group of inherited rare diseases.

Introduction

The liaison between muscular dystrophy and heart dysfunction is well known in medical genetics. More than 90 muscular dystrophy phenotypes have been identified, of which the majority also display cardiac manifestations (1–3). Both dilated cardiomyopathies and cardiac arrhythmia phenotypes are often found as comorbidities and may even precede the onset of the muscle symptoms (4–6). The limb-girdle muscular dystrophies (LGMDs) are inherited diseases with onset after birth and are characterized by progressive weakness and muscle atrophy predominantly affecting the hips, shoulders, and proximal extremity muscles (3). There are both autosomal dominant (LGMD1) and autosomal recessive (LGMD2) subtypes known. Today, a total of 31 different LGMD loci have been identified (7). A variety of mutations are known in the corresponding genes, which belong to several different cellular pathways, including sarcolemmal glycoproteins (dystroglycan and sarcoglycans), scaffolding proteins (caveolin-3 [CAV3]), and proteins involved in membrane repair and vesicle trafficking (dysferlin [DYSF] and anoctamin-5 [ANO5]) (7).

POPDC1, which is also known as *BVES*, is a member of the Popeye domain–containing (*Popdc*) gene family, encoding transmembrane proteins, which is highly expressed in cardiac and skeletal muscle in an overlapping manner (8, 9). POPDC proteins possess the evolutionarily conserved Popeye domain, which functions as a high-affinity cAMP-binding site (8, 10). POPDC proteins are localized primarily at the plasma membrane and in t-tubules (10), although they have also been found at the nuclear envelope of striated muscle cells (11). An interaction of POPDC proteins with CAV3 and the 2-pore domain potassium channel TREK-1 has been reported (10, 12). In the presence of POPDC proteins, TREK-1 cur-

Authorship note: R.F.R. Schindler, C. Scotton, and J. Zhang contributed equally to this work. J. Wang, T. Brand, and A. Ferlini are co-senior authors.
Conflict of interest: The authors have declared that no conflict of interest exists.
Submitted: October 31, 2014; **Accepted:** October 29, 2015.
Reference information: *J Clin Invest*. 2016;126(1):239–253. doi:10.1172/JCI79562.

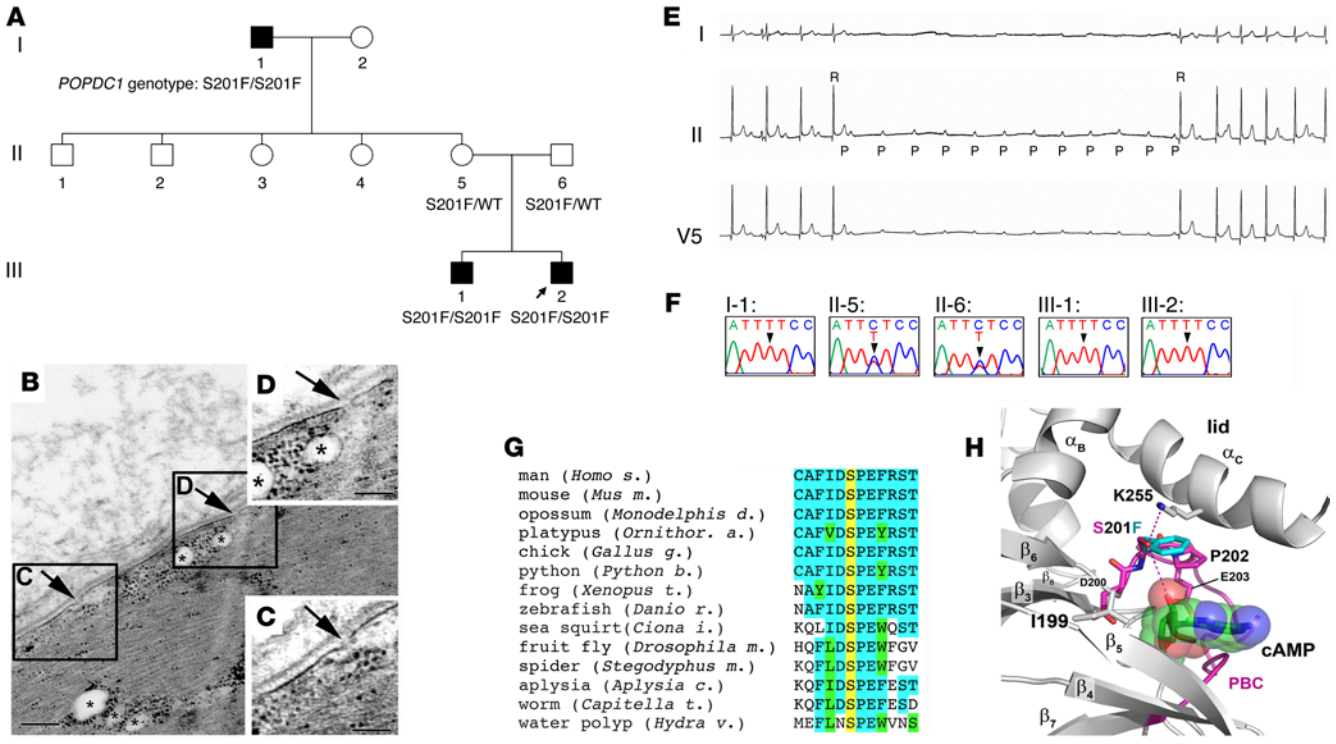

Figure 1. Identification of the *POPDC1*^{S201F} mutation associated with AV block and LGMD. (**A**) Pedigree of a family homozygous for the *POPDC1*^{S201F} mutation. The index patient (PTIII-2) and his brother (PTIII-1) suffered from AV block and the grandfather (PTI-1) from LGMD and AV block. (**B**) TEM analysis of skeletal muscle of PTI-1 revealed the presence of plasma membrane discontinuities (arrows) and subsarcolemmal and intermyofibrillar vacuoles (asterisks). **C** and **D** show higher magnifications of the boxed areas in **B**. Scale bars: 2 μm (**B**); 1 μm (**C** and **D**). Data depicted are representative of results derived from a single biopsy. (**E**) Holter ECG of the index patient (PTIII-2) displaying an episode of a paroxysmal AV block. (**F**) Electropherogram of the Sanger sequencing of genomic DNA isolated from family members. (**G**) Sequence alignment of part of the Popeye domain demonstrating sequence conservation. Many residues are identical (turquoise) or similar (green); however, S^{201} (yellow) is ultraconserved. (**H**) 3D model of the Popeye domain. Only the phosphate-binding cassette (PBC) is shown. Two hydrogen bonds are formed by S^{201}, but these are lost when the F^{201} (turquoise) mutant residue is present, possibly affecting the ligand-binding affinity of the Popeye domain.

rents are potentiated due to enhanced membrane trafficking (10). The *Popdc1* null mutant in mice displays a retardation of muscle regeneration (13). Moreover, an impaired recovery from cardiac ischemia and an increase in infarct size have been described in the *Popdc1* null mutant (12). Both *Popdc1* and *Popdc2* null mutants display a stress-induced sinus node bradycardia, which develops in an age-dependent manner (10, 14). In zebrafish, *popdc2* morphants develop embryonic heart failure, atrioventricular (AV) block, and muscular dystrophy (15). Thus, both heart and skeletal muscle pathologies have been associated in model organisms with the loss of either *Popdc1* or *Popdc2*. However, so far, *Popdc* genes have never been associated with human hereditary diseases.

We report here the identification of a homozygous recessive mutation in *POPDC1* (c.602C>T, p.S201F) by whole-exome sequencing (WES) in a family with LGMD and AV block. We demonstrate that POPDC1^{S201F} has strong pathogenic consequences, since it affects cAMP binding and subcellular localization of the mutant protein and its interaction partners. Therefore *POPDC1* is a disease-causing gene associated with LGMD and cardiac arrhythmia.

Results

POPDC1 is a disease-causing gene associated with cardiac disturbances and LGMD. A family originating from a small Albanian enclave town of about 3,000 inhabitants located in Calabria (Italy) showed an interesting pseudodominant inheritance, compatible with consanguinity and geographic isolation (Figure 1A). The grandfather, 81 years old at the time of writing (PTI-1), started to complain of lower limb-girdle weakness around the age of 40 and lost the ability to walk without aids around the age 60. At that time, blood creatine kinase (CK) was elevated (range, 750–1300 IU/l). At the age of 60, a muscle biopsy was performed in his left deltoid muscle showing muscular dystrophy changes, with diameter variability, increased central nuclei, and the presence of a few necrotic and regenerating fibers (Supplemental Figure 1; supplemental material available online with this article; doi:10.1172/JCI79562DS1). Transmission electron microscopy (TEM) analysis revealed the presence of plasma membrane discontinuities and submembraneous vacuoles (Figure 1, B–D). Expression of dystrophin (DYS), all sarcoglycans, emerin, merosin, and CAV3 was normal (data not shown). At age 59, this patient started to complain of repeated syncope episodes, and a second-degree AV block was disclosed. A pacemaker was placed 1 year later at the age of 60. Echocardiography excluded a cardiomyopathy. Muscle testing at the age of 72 showed a clear symmetrical weakness of the limbs (neck flexors Medical Research Council Scale for Muscle Strength [MRC] 5; ileopsoas MRC 3.5; quadriceps MRC 2; glutei MRC 1; gastrocnemius MRC 5; foot

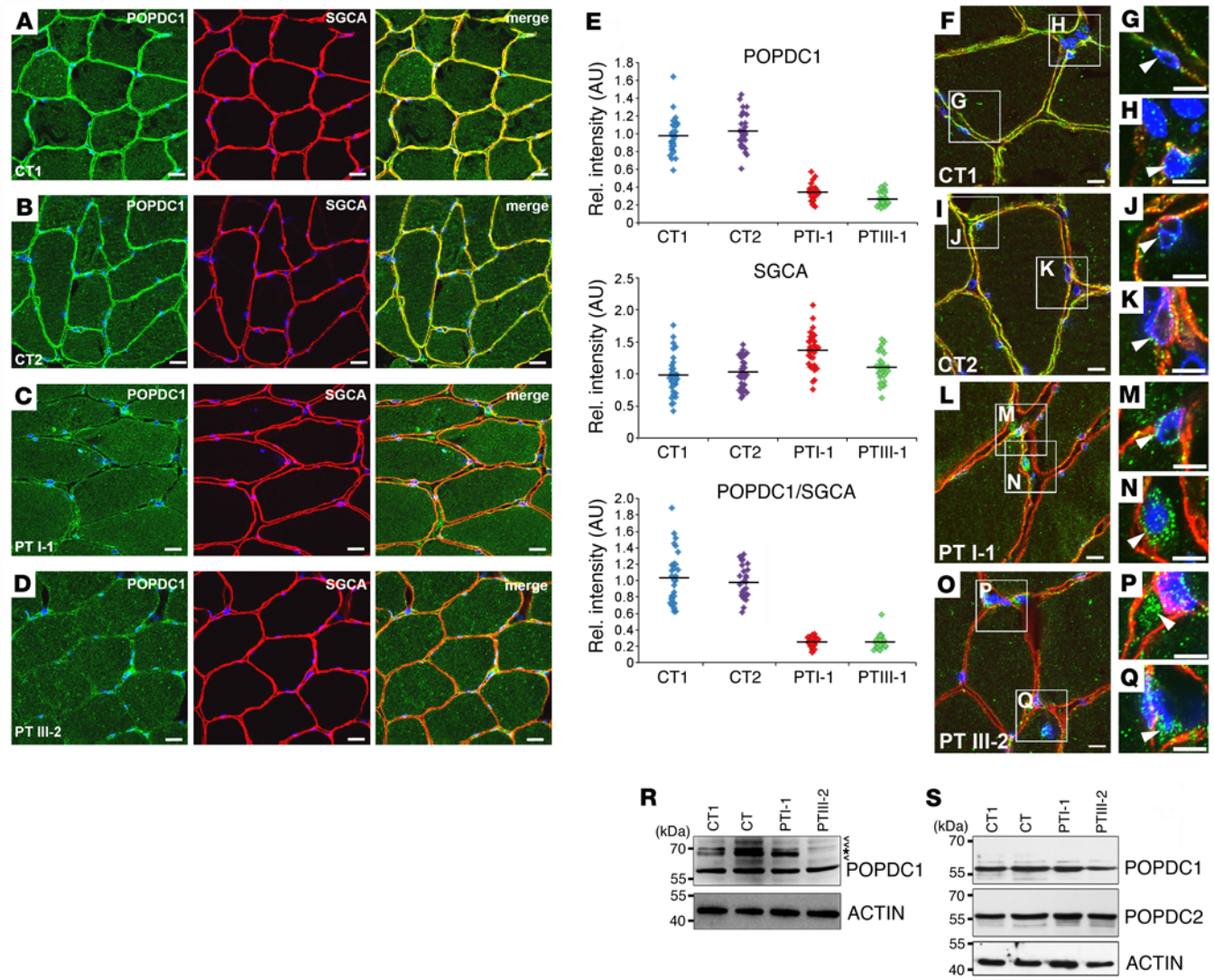

Figure 2. Membrane trafficking of POPDC1 is affected in muscle biopsies. Skeletal muscle biopsies of PTI-1 and PTIII-1 and 2 controls were immunostained for (**A**–**D**) POPDC1 (green signal) and SCGA (red signal). (**E**) The immunofluorescence signals were quantified in 10 muscle fibers of 3 sections per biopsy. The signals of POPDC1 and SGCA and the ratio of both were plotted relative to the means of both controls, which were set at 1. (**F**–**Q**) Subcellular localization of POPDC1 in (**F**–**H**) CT1, (**I**–**K**) CT2, (**L**–**N**) PTI-1, and (**O**–**Q**) PTIII-2. Perinuclear localization of POPDC1 is only weakly present in control samples, whereas in patients' muscle biopsies, a significant perinuclear accumulation of the mutant protein was seen. Scale bars: 10 μm (**A**–**D**, **G**, **H**, **J**, **K**, **M**, **N**, **P**, and **Q**); 20 μm (**F**, **I**, **L**, and **O**). (**R** and **S**) Western blot analysis of (**R**) POPDC1 expression in skeletal muscle biopsies and of (**S**) POPDC1 and POPDC2 in dermal fibroblasts of 2 controls (CT1 and CT2) and PTI-1 and PTIII-2. The main POPDC1 isoform in **R** is labeled by POPDC1. Additional isoforms are indicated by arrows, while bands, which are considered to be unspecific and remain present after peptide competition (Supplemental Figure 4, A and B), are indicated by an asterisk. Results are representative of 3 independent experiments.

dorsal flexors MRC 5). The grandfather had 2 healthy sons and 3 healthy daughters. One of the daughters had 2 children showing the same phenotype as the grandfather, although apparently both parents denied consanguinity. The eldest son (PTIII-1), 25 at the time of this writing, started to manifest syncopal episodes during exercise at the age of 17, and his CK level was elevated to 1216 IU/l. The electrocardiogram at that age showed a second-degree AV infra-Hisian block with no aberrant intraventricular conduction and negative response to intravenous flecainide. Holter monitoring revealed episodes of paroxysmal second-degree AV block (Mobitz 2) (Figure 1E and Supplemental Figure 2, A–C). Echocardiography was normal. An endocardial double-chamber pacemaker was implanted. The muscle CT scan was normal (Supplemental Figure 3A). Muscle biopsy was proposed and refused by the patient. The younger brother (PTIII-2) started to complain of syncope episode with facial trauma at the age of 12 years. At that age, the CK level was elevated to 7643 IU/l after prolonged exercise and to 3182 IU/l at rest. During hospitalization, the ECG was normal and Holter monitoring showed occasional episodes of second-degree AV block (Mobitz 1) (Supplemental Figure 2, D–F). The head-up tilt test showed sinus bradycardia and escape junctional rhythm in the absence of symptoms. Echocardiography was normal, excluding a cardiomyopathy. The endocavitary electrophysiological study documented a normal His bundle–ventricle (HV) interval (30 ms) and an advanced infranodal AV block during atrial pacing at a cycle length of less than 600 ms. For these reasons, a single-chamber

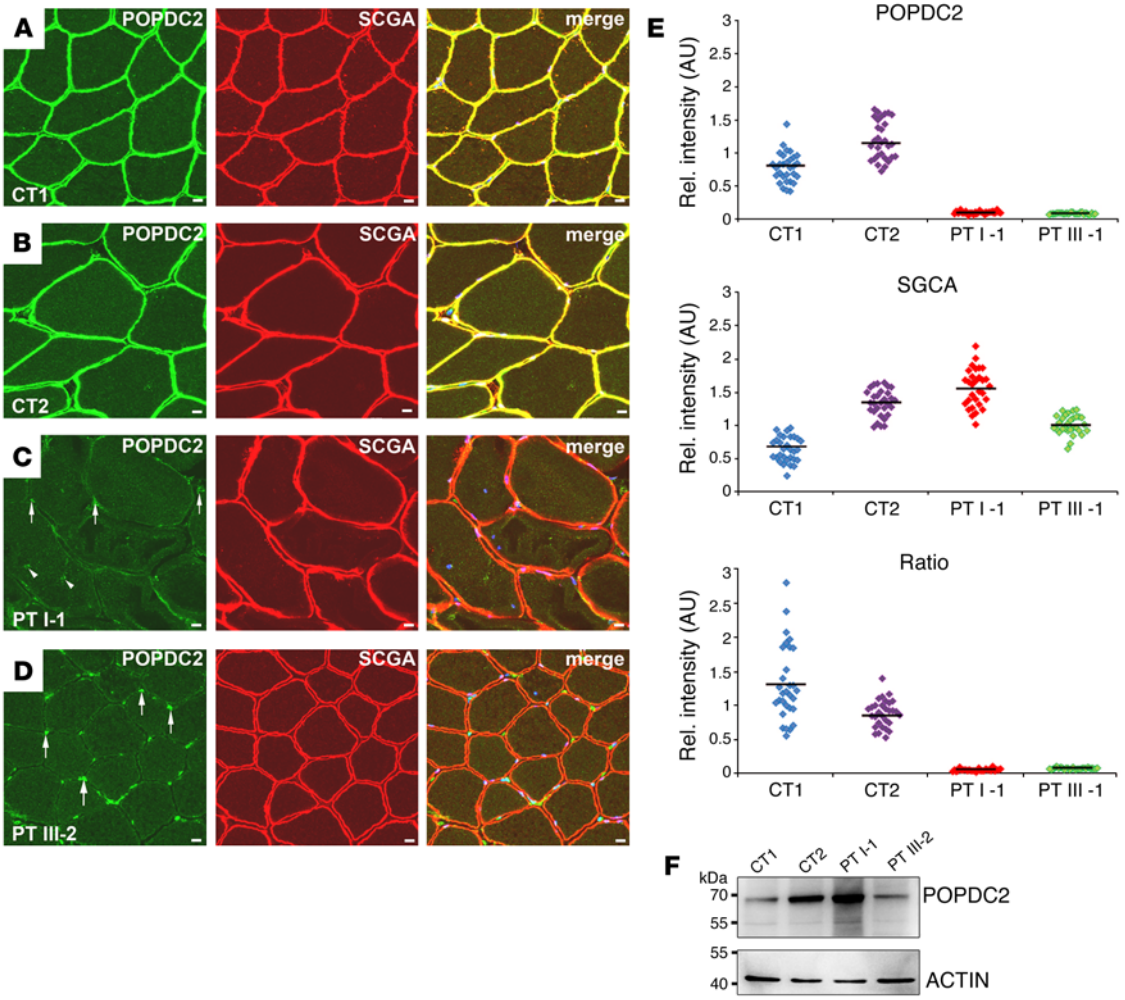

Figure 3. Membrane trafficking of POPDC2 is affected in patients with a homozygous POPDC1^{S201F} mutation. Skeletal muscle biopsies of PTI-1 and PTIII-2 and 2 controls were immunostained for (**A**–**D**) POPDC2 (green signal) and SCGA (red signal). (**E**) Quantification of the relative intensities of the plasma membrane staining of POPDC2 and SGCA in 10 fibers each from 3 sections per biopsy. The signals of POPDC2 and SGCA and the ratio of both were plotted relative to the means of both controls, which were set at 1. The normalized intensities revealed a downregulation of the membrane localization of POPDC2 in the patient material. Scale bars: 10 μm. (**F**) Western blot analysis of POPDC2 expression in the muscle biopsy material of the 2 controls (CT1 and CT2) and PTI-1 and PTIII-2. Results are representatives of 3 independent experiments.

endocardial (VVI) pacemaker was implanted, which after 8 years was upgraded to a double-chamber pacemaker. The muscle biopsy was normal (data not shown), and a CT scan at the age of 19 years did not show skeletal muscle involvement despite a very high CK level (Supplemental Figure 3B). At the time of this writing, the patient was being periodically checked and had not shown further episodes of syncope or other symptoms.

Using WES, we identified in this family a homozygous missense mutation (c.602C>T, p.S201F) in *POPDC1*. The S201F variant has not been reported in any of the known databases, such as dbSNP (16), 1000 Genomes (17), the NHLBI Exome Sequencing Project (18), and the ExAC Database (19). This variation was shared in homozygosis in PTIII-1 and PTIII-2 (Figure 1F). Sanger sequencing validated the c.602C>T SNP and confirmed that it was present in homozygosis in the 2 sons and their grandfather (PTI-1) and in heterozygosis in both nonaffected parents (PTII-5 and PTII-6) as expected for a pseudodominant inheritance due to inbreeding in the family. Further screening of 104 patients with a similar clinical phenotype gave a negative result, suggesting this mutation to be very rare and family specific (Supplemental Table 1). The S201F mutation is located within the Popeye domain, which is the most conserved part of POPDC1 and functions as a cAMP-binding domain (10). S201 is a residue of the ultraconserved DSPE motif, which is thought to be part of the phosphate-binding cassette (Figure 1G and refs. 9, 10, 14). In a 3D model of the Popeye domain (10), S201 is predicted to be localized to the nucleotide-binding region facing the cyclic AMP molecule, and its hydroxyl group might possibly engage via hydrogen bonding either with the 2′-hydroxyl group of the ribose ring or the side chain amine group of K255, which is located in the lid helix αC and potentially controls the allosteric transfer of cAMP binding (Figure 1H). In the S201F protein model, the aromatic side chain of the introduced phenylalanine protrudes into the cAMP-binding pocket, thereby likely impairing cyclic nucleotide binding and exchange.

The S201F mutation affects membrane trafficking of both POPDC1 and POPDC2. In healthy skeletal muscle fibers, POPDC1 and

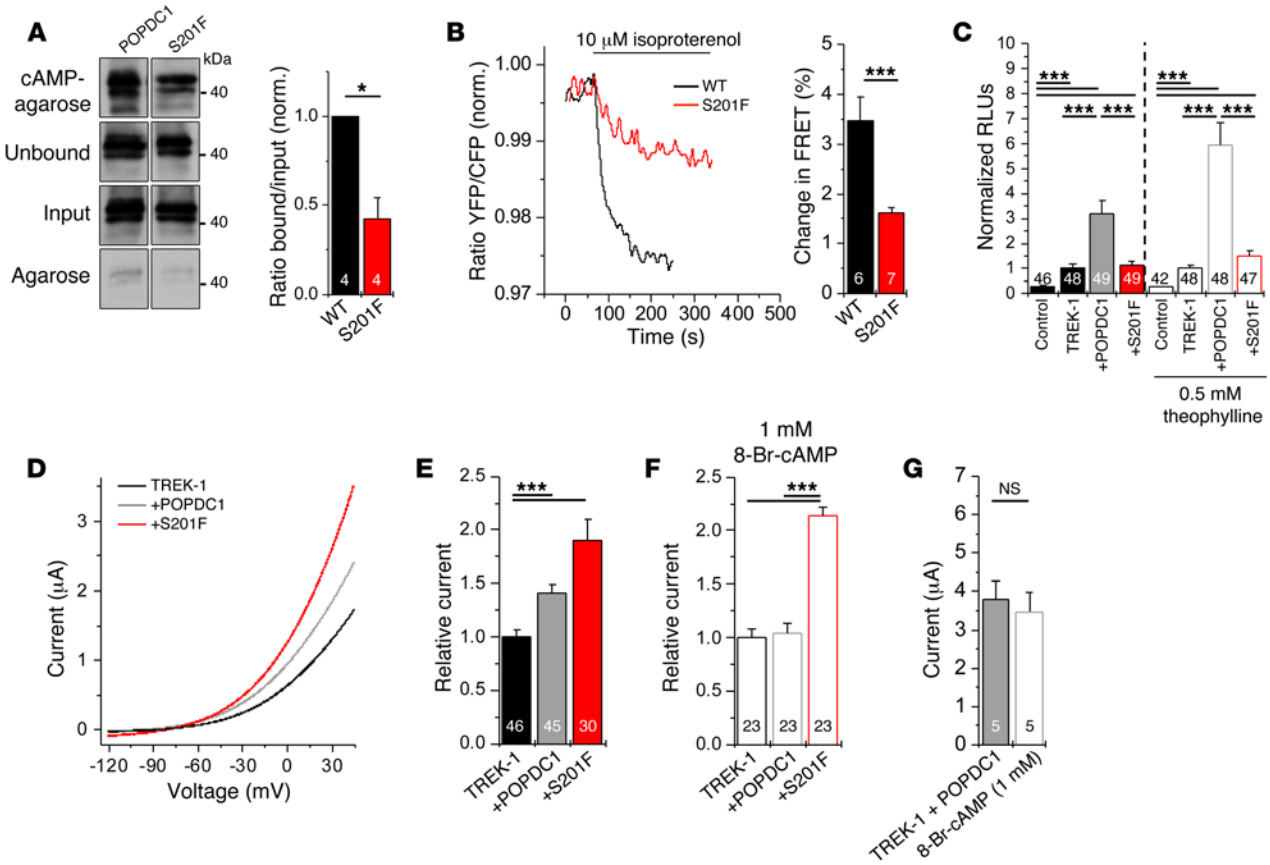

Figure 4. The POPDC1^{S201F} mutant protein displays a reduced cAMP affinity. (**A**) cAMP affinity precipitation of WT or POPDC1^{S201F} protein. Left panel: precipitated proteins, unbound fraction, and input samples as well as protein subjected to control precipitation using ethanolamine-agarose (agarose) were subjected to Western blot detection of POPDC1. Right panel: quantification of cAMP affinity, calculating the ratios between input and cAMP agarose–bound protein fractions. (**B**) Left: example of a FRET measurement of 293A cells transfected with YFP–TREK-1 together with POPDC1-CFP or POPDC1^{S201F}-CFP. Right: relative change in FRET signal as a measure of cAMP affinity. (**C**) Chemiluminescence assay in *Xenopus* oocytes analyzing the surface expression of extracellularly HA-tagged TREK-1 in the absence or presence of POPDC1 or POPDC1^{S201F}. Control, noninjected oocytes. Measurements after incubation with 0.5 mM theophylline are illustrated with white bars. (**D**) Representative 2-electrode voltage clamp measurements in oocytes injected with TREK-1 alone (black) or coinjected with Popdc1 (gray) or POPDC1^{S201F} (red). Voltage was ramped from –110 to +35 mV. (**E**) Relative current amplitudes at 0 mV. (**F**) 2-Electrode voltage clamp measurements in oocytes injected with TREK-1 or coinjected with POPDC1 or POPDC1^{S201F} bathed after cRNA injection in a storage solution containing 1 mM 8-Br-cAMP. (**G**) Relative current amplitudes of TREK-1 coinjected with POPDC1, measured in recording solution or directly after 10 minutes of perfusion with 2 mM 8-Br-cAMP. (**A**–**C** and **E**–**G**) Numbers of experiments are included in the bars. Results are presented as mean ± SEM. Two groups of measurements in **A** were compared by paired 2-tailed Student's *t* test. One-way ANOVA was used for the data presented in **B**, **C**, and **E**–**G**. $^{*}P < 0.05$; $^{***}P < 0.001$.

POPDC2 were prominently expressed in the sarcolemma (Figure 2, A, B, E, and Figure 3, A, B, and E). In contrast, in skeletal muscle biopsies of PTI-1 and PTIII-2, a significant reduction in membrane localization of both POPDC1 and POPDC2 was observed (Figure 2, C–E, and Figure 3, C–E). While plasma membrane labeling was diminished, an increased perinuclear localization of POPDC1 and POPDC2 was observed in the patients' biopsies (Figure 2, F–Q, and Figure 3, C and D). In addition, pronounced expression in cells adjacent to the muscle fiber, which may represent activated satellite cells or myoblasts, was observed and particularly prominent in cases of POPDC2 in both patients (Figure 3, C and D). The total levels of POPDC1 and POPDC2 in muscle biopsies and in dermal fibroblast were determined by Western blot analysis (Figure 2, R and K, Supplemental Figure 3, and Supplemental Figure 4). The expression levels varied slightly between samples; however, total protein levels did not correlate with the significant reduction of the plasma membrane levels of POPDC1 and POPDC2 in the patients' muscle fibers, suggesting that the S201F mutation predominantly causes a reduction in plasma membrane trafficking rather than affecting protein expression levels.

The histological analysis and CT scan demonstrated absence of severe fibrosis and fat replacement in PTIII-1 and PTIII-2 (Supplemental Figure 1, A–C, and Supplemental Figure 3). However, in the grandfather (PTI-1), fiber size variability, central nuclei, and plasma membrane discontinuities in muscle fibers were observed (Figure 1E and Supplemental Figure 1D). TEM of PTIII-2 failed to detect membrane discontinuities or any other abnormality of the caveolae, basal membrane, and nuclear pores (data not shown), which is in accordance with the late onset of muscle pathology in this family. We studied the expression of proteins involved in membrane stability and repair in PTI-1 and PTIII-2 in comparison with 2 controls (Supplemental Figures 5–9). We previously reported protein-protein interaction of POPDC1 with CAV3 (12). However, the membrane presence of CAV3 was not altered in the patients'

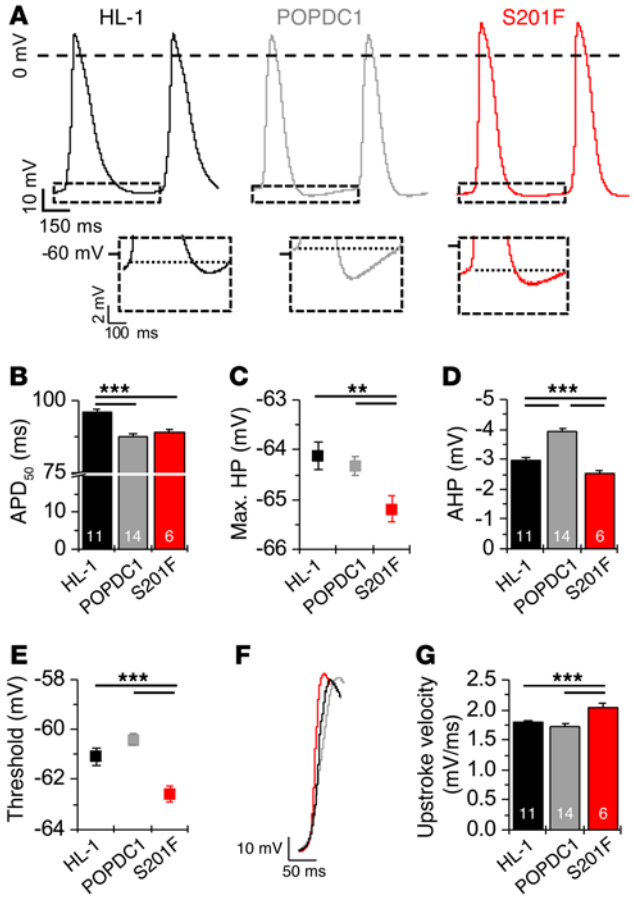

Figure 5. POPDC1^{S201F} hyperpolarizes the membrane potential of spontaneously beating HL-1 cells. (**A**) Representative action potentials recorded for HL-1 cells or HL-1 cells transfected with POPDC1 or POPDC1^{S201F}. The boxes at the bottom represent an enlarged view to show the effects on maximal hyperpolarization and afterhyperpolarization. (**B**) Analyses of the action potential duration, analyzed at 50 % of repolarization (APD_{50}). (**C**) Analyses of maximal hyperpolarization (Max. HP), (**D**) afterhyperpolarization (AHP), and (**E**) activation threshold for HL-1 cells or HL-1 cells transfected with POPDC1 or POPDC1^{S201F}. (**F**) Enlarged view showing the upstroke phase of an action potential of HL-1 cells or HL-1 cells transfected with POPDC1 or POPDC1^{S201F}. Traces were aligned to the activation threshold. (**G**) Analyses of the upstroke velocity (Up. vel.). Results are presented as mean ± SEM. One-way ANOVA was used to compare multiple variables presented in **B**–**E** and **G**. $^{**}P < 0.01$; $^{***}P < 0.001$.

muscle biopsies in comparison with controls (Supplemental Figure 5). We also studied DYS, which was coimmunoprecipitated with POPDC1 (Supplemental Figure 6). However, we could not detect any difference in membrane localization between patient and control samples (Supplemental Figure 7). Membrane discontinuities were observed in the muscle biopsy of the grandfather (PTI-1), a feature that is typical of dysferlinopathies and related muscle disorders (20, 21). We established association of DYSF with POPDC1 by colocalization and coimmunoprecipitation (Supplemental Figure 8). However, plasma membrane levels of DYSF were not affected in patients with a homozygous POPDC1^{S201F} mutation (Supplemental Figure 9). These data indicate that POPDC1 does not affect sarcolemmal localization of DYS, DYSF, and CAV3. Possibly, these protein-protein interactions only become essential under particular physiological conditions, such as in response to membrane wounding or during muscle regeneration (13).

The POPDC1^{S201F} mutant protein displays a reduction of its affinity for cAMP. The S201 residue is part of the ultraconserved DSPE motif, which is essential for cAMP binding (10). We therefore assessed whether the change of serine to phenylalanine might cause a reduction in cAMP affinity of POPDC1 with the help of a ligand precipitation assay, previously utilized for the mouse protein (10). We found that the S201F mutant protein has an approximately 50% reduction in affinity for cAMP (Figure 4A). To corroborate this finding, we employed a bimolecular fluorescence resonance energy transfer (FRET) sensor based on the interaction of POPDC1 and TREK-1, analogous to what was previously described for mouse POPDC1 (10). FRET was observed after cotransfection of either CFP-tagged WT POPDC1 or POPDC1^{S201F} together with YFP–TREK-1. Upon stimulation with isoproterenol (Iso) or forskolin, a small but robust decrease of the FRET ratio was observed for WT POPDC1, but changes in the case of POPDC1^{S201F} were much weaker (~50%), confirming in an independent assay the decreased cAMP sensitivity of the POPDC1^{S201F} mutant (Figure 4B and Supplemental Figure 10). No decrease of the FRET ratio was observed when the cotransfected cells were preincubated with propranolol prior to Iso stimulation, demonstrating that the Iso-induced change in FRET ratio represented a β-adrenergic receptor–dependent event (Supplemental Figure 10).

To demonstrate that the different response to rising cAMP levels of mutant and WT POPDC1 is based on different cAMP affinities and not due to an impaired interaction between POPDC1^{S201F} and TREK-1, we narrowed down the TREK-1 interaction domain using the mouse protein by deletion and coimmunoprecipitation analysis (Supplemental Figure 11). The interaction with POPDC1 was lost when 219 amino acids were deleted from the carboxy terminus. These data suggest that the TREK-1 interaction domain of POPDC1 is located between residues 139 and 186 and therefore is positioned at some distance from the phosphate-binding cassette (residues 198–218). Consequently, it is unlikely that the S201F mutation directly affects the interaction of POPDC1 with TREK-1. This conclusion is also supported by the observation that both mutant and WT POPDC1 colocalize with TREK-1 after cotransfection (Supplemental Figure 12).

Enhanced surface expression of TREK-1 by POPDC1 is lost by the S201F mutation. Enhanced TREK-1 outward currents are observed after coexpression of mouse POPDC1 and TREK-1 in *Xenopus* oocytes (10). For mouse POPDC2, we were able to establish that the increased outward current of TREK-1 is most likely caused by an enhanced surface expression of the channel (10). Here, we show that the coexpression of TREK-1 with human POPDC1 also caused strongly increased surface expression of the channel (Figure 4C). Interestingly, the S201F mutation impaired the ability of POPDC1 to enhance the surface expression of TREK-1 (Figure 4C). Moreover, raising intracellular cAMP levels by the phosphodiesterase inhibitor theophylline resulted in an almost 6-fold increase in surface expression of TREK-1 when coexpressed with WT POPDC1. However, in the presence of the S201F mutant, the surface expression of TREK-1 was not affected (Figure 4C). Thus, similar to the impaired plasma membrane localization of POPDC2 in the patients' mus-

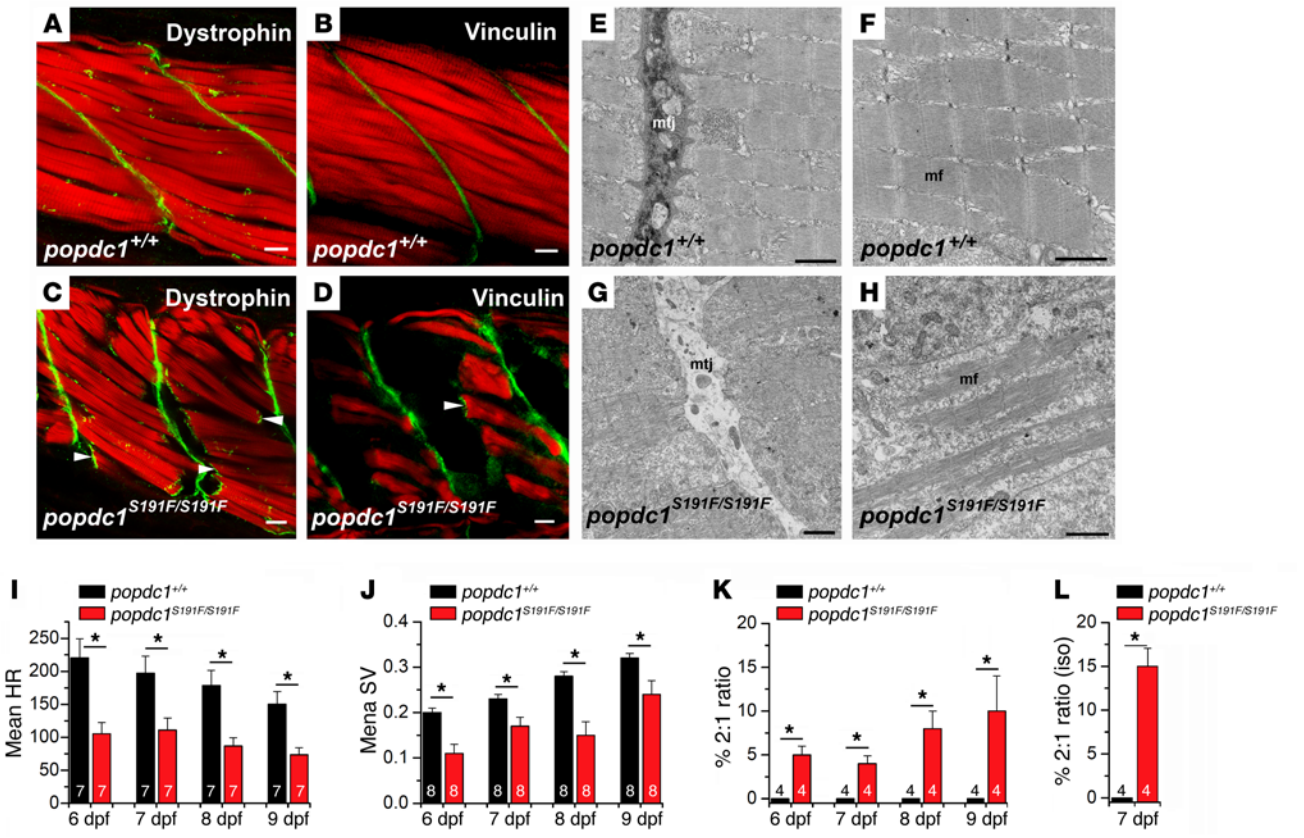

Figure 6. The *popdc1*^{S191F} zebrafish mutant displays muscular dystrophy and cardiac arrhythmia. (**A**–**D**) Confocal analysis of actin (phalloidin staining, red channel) and (**A** and **C**) DYS (green channel) or (**B** and **D**) vinculin (green channel) expression in trunk skeletal muscle of (**A** and **B**) WT (*popdc1*$^{+/+}$) and (**C** and **D**) homozygous mutants (*popdc1*$^{S191F/S191F}$). Lateral view of the tail musculature in larvae at 5 dpf. Homozygous mutants develop lesions in skeletal muscle. Muscle fibers detach from the MTJ and retract. Arrowheads indicate the presence of DYS and vinculin immunoreactivity at the end of the ruptured fibers, suggesting that the fibers that have lost connection to the MTJ are probably physically intact. The results shown are representative of 3 independent experiments. (**E**–**H**) TEM analysis of trunk skeletal muscle of (**E** and **F**) WT and (**G** and **H**) homozygous *popdc1*^{S191F} 5-dpf mutant zebrafish embryos. The MTJ in the homozygous mutant is characterized by a lack of electron-dense material. The results shown are representative of 3 independent experiments. (**I**–**L**) Analysis of heart function in WT and homozygous *popdc1*^{S191F} mutant embryos. (**I**) Mean heart rate (HR). (**J**) Mean stroke volume. (**K**) Percentage of embryos displaying a 2:1 AV block. (**L**) Percentage of embryos displaying a 2:1 AV block after Iso stimulation. Number of embryos in each group is indicated on the corresponding bar plot. Results are presented as mean ± SEM. Two groups of measurements in parts **I**–**L** were compared by paired 2-tailed Student's *t* test. $^*P < 0.05$. Scale bars: 10 μm (**A**–**D**); 1 μm (**E** and **F**); 2 μm (**G** and **H**). mf, myofibrils.

cle biopsies, membrane trafficking of TREK-1 in *Xenopus* oocytes was affected in the presence of the S201F mutant. Coexpression of TREK-1 with POPDC1 led to increased current amplitudes for both WT and mutant S201F (Figure 4, D and E). Surprisingly, coexpression of the S201F mutant with TREK-1 caused an even more pronounced enhancement of TREK-1 outward currents than WT POPDC1. While POPDC1 increased TREK-1 currents by 40%, the S201F mutant caused an increase of the TREK-1 current by 90%. Thus, despite the inability of augmenting TREK-1 surface expression, the S201F mutant was able to enhance TREK-1 outward currents, which was presumably caused by an increased conductivity of the channels in complex with POPDC1^{S201F}. In the presence of the membrane-permeable cAMP analog 8-Br-cAMP, the effects of WT POPDC1 on TREK-1 currents were basically abolished (Figure 4F). Thus, irrespective of the surface expression, increased cAMP levels neutralized the impact of POPDC1 on TREK-1 conductivity (Figure 4C). Interestingly, perfusion of the oocytes expressing TREK-1 in complex with POPDC1 with 8-Br-cAMP (1 mM) during 2-electrode voltage-clamp recordings did not affect TREK-1 current amplitudes (Figure 4G), indicating that the altered conductivity of the TREK-1/POPDC1 complex is not mediated by a pure gating effect (cAMP switch) (9). Most importantly, and consistent with a reduced cAMP sensitivity of the mutant protein, POPDC1^{S201F} retained the ability to enhance TREK-1 currents even in the presence of 8-Br-cAMP (Figure 4F). Thus, despite the inability of POPDC1^{S201F} to affect the surface expression of TREK-1 (Figure 4C), the mutant protein caused increased TREK-1 outward currents. These seemingly opposing effects of the S201F mutant protein to cause impaired channel trafficking while enhancing gating may explain to some extent the cardiac arrhythmia phenotype in the patients.

Forced expression of POPDC1^{S201F} *hyperpolarizes the membrane potential of spontaneously beating HL-1 cells.* Since POPDC1 is predominantly expressed in striated muscle cells, we used HL-1 cells, which are spontaneously beating sinoatrial node-like myocytes (22), to probe for changes in cellular electrophysiology by forced expression of the POPDC1^{S201F} mutant. Both POPDC1 and POPDC2 are endogenously expressed in HL-1 cells and are membrane localized (Supplemental Figure 13). We transfected

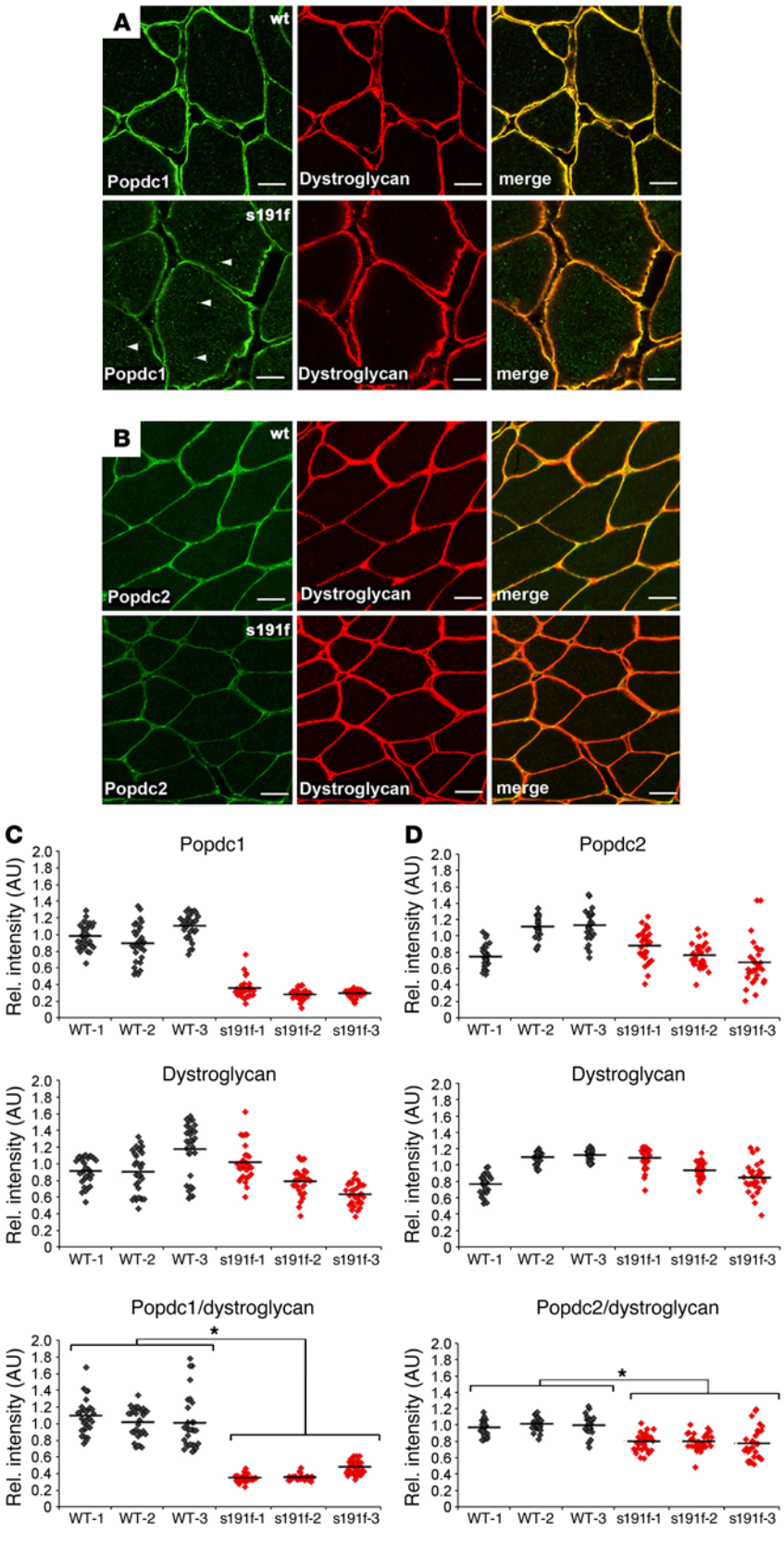

Figure 7. Expression of Popdc1 and Popdc2 in the trunk skeletal muscle of the adult zebrafish. (**A** and **B**) Transversal sections through the trunk skeletal muscles of WT (*popdc1*$^{+/+}$) and homozygous *popdc1*^{S191F} mutants (*popdc1*$^{S191F/S191F}$) were stained with antibodies for α-dystroglycan and (**A**) Popdc1 or (**B**) Popdc2. Scale bars: 10 μm. (**C** and **D**) Quantification of the plasma membrane staining of (**C**) Popdc1 and (**D**) Popdc2 in WT and homozygous Popdc1^{S201F} mutant animals, respectively. The regions of interest of 30 fibers were analyzed for each sample. The membrane localization of both Popdc1^{S191F} and Popdc2 is reduced in the *popdc1*$^{S191F/S191F}$ mutants. In agreement with the reduction in plasma membrane localization, increased amounts of the Popdc1^{S191F} mutant protein are found in cytoplasmic vesicles (arrowheads in **A**). For statistical testing, mean values of the Popdc/dystroglycan ratios of WT (n = 3) and mutants (n = 3) were compared by paired 2-tailed Student's t test (**C** and **D**). *P < 0.05.

CFP-tagged WT POPDC1 or POPDC1^{S201F} in HL-1 cells and recorded action potential properties of spontaneously beating cells using patch-clamp experiments. Forced expression of WT POPDC1 into HL-1 cells resulted in a pronounced afterhyperpolarization (Figure 5, A and D) and shortening of the action potential duration (Figure 5, A and B) compared with nontransfected HL-1 cells. These results are well in agreement with the overexpression of a TREK-1–activating protein in HL-1 cells, as these cells contain endogenous TREK-1 channels (Supplemental Figure 14). Most importantly, transfecting the same amount of POPDC1^{S201F} and TREK-1 cDNA caused a hyperpolarization of the maximal diastolic membrane potential (Figure 5, A and D). This effect is in agreement with a more pronounced activation of TREK-1 channels by POPDC1^{S201F} (Figure 4, D and E). As cells with POPDC1^{S201F} were more hyperpolarized (Figure 5C) and the activation threshold was also shifted to more negative membrane potentials (Figure 5E), there was a reduced afterhyperpolarization compared with WT POPDC1 (Figure 5D). The more hyperpolarized maximal diastolic membrane potential might lead to an increased availability of sodium channels in these cells (23, 24). This assumption is in agreement with the observation of a more hyperpolarized activation threshold (Figure 5E) and the increased upstroke velocity (Figure 5,F and G) in HL-1 cells transfected with POPDC1^{S201F}. In summary, the overexpression experiments in HL-1 cells demonstrate that the mutant is more efficient than WT protein at raising potassium conductance in these

cardiac myocyte-like cells, leading to increased hyperpolarized membrane potentials. These effects might explain the AV block observed in patients and in the POPDC1^{S191F} zebrafish mutant (see below), as hyperpolarization of cells in the AV node will further delay the propagation of excitation to the ventricles.

Loss of popdc1 in zebrafish causes an impairment of heart and skeletal muscle development. Zebrafish *popdc1* is expressed in both skeletal muscle and heart (Supplemental Figure 15, A–C). To assess *popdc1* function in zebrafish, a morpholino-based knockdown approach targeting the splice junctions of exon 4 was utilized. Morpholino injection caused a significant reduction of *popdc1* mRNA expression (Supplemental Figure 15D). Macroscopically, the morphants appeared normal overall, with the exception of the presence of a cardiac edema in a large fraction of the injected embryos (70%) (Supplemental Figure 15, E and F). Some morphants (20%) displayed a 2:1 AV block, a phenotype that has been previously reported for *popdc2* morphants (Supplemental Figure 15G, Supplemental Videos 1 and 2, and ref. 15). Upon closer inspection, skeletal muscle was also affected in 80% of the morphants and was characterized by myofibrillar misalignment and fiber detachment (Supplemental Figure 15H). The myotendinous junction (MTJ) forms the attachment site for muscle fibers, and was found to be malformed in the morphants and possibly the cause for the fiber detachment (25). Forced expression of mutant and WT POPDC1 was achieved by mRNA injection into fertilized zebrafish eggs. WT POPDC1 did not affect cardiac morphology; however, forced expression of POPDC1^{S201F} caused myocardial edema formation indicative of embryonic heart failure (Supplemental Figure 16, A and B).

In order to directly test the pathogenicity of the POPDC1^{S201F} mutation, we generated by TALEN-mediated gene editing a genomic mutation of the corresponding serine residue in zebrafish *popdc1* (i.e., *popdc1*^{S191F}). The homozygous *popdc1*^{S191F} mutant developed normally during embryogenesis, and no significant lethality in comparison with WT embryos was observed (data not shown). However, a significant fraction of homozygotes developed cardiac and skeletal muscle phenotypes (Supplemental Figure 17). Mutants displayed cardiac edema and aberrant formation of the trunk musculature, and, in the most severely affected embryos, an edema involving the entire larval body was observed. The mutant phenotype displayed a reduced penetrance of approximately only one-third of the embryos, which appeared to be affected at 5 days post fertilization (dpf). Thus, a majority of homozygotes developed into adulthood. One of the reasons for the reduction in phenotype penetrance was the presence of 3 family members that at least partially were able to functionally substitute for each other (9).

In order to further study the skeletal muscle phenotype, zebrafish larvae at 5 dpf were stained with phalloidin together with vinculin or DYS. The trunk skeletal muscle of some homozygous *popdc1*^{s191f} mutants displayed myofibrillar misalignment, aberrant formation of the MTJ, and myofiber detachment, probably secondary to the impaired MTJ formation, with various degrees of severity (Figure 6, A–D). Myofiber detachment is a hallmark of muscular dystrophy phenotypes in zebrafish and was previously reported, for example, for the DYS mutant *sapje* (26). TEM of trunk muscle development in the homozygous *popdc1*^{s191f} mutant demonstrated an almost complete absence of extracellular matrix (ECM) in the MTJ at 5 dpf (Figure 6, E and G). In addition to the MTJ phenotype, a severe reduction in myofibrillar content and disarray was also observed (Figure 6, F and H).

We assessed cardiac performance using optical recording, which revealed an overall reduction in heart rate and stroke volume (Figure 6, I and J). Between 5 dpf and 9 dpf, a steadily increasing number of homozygotes developed a 2:1 AV block (Figure 6K). In addition, more severe forms of AV block such as 3:1 and even longer pauses including electrically silent ventricles were also observed in homozygotes (Supplemental Figure 18 and Supplemental Video 3). The arrhythmia phenotype displayed a reduced penetrance, with approximately 5%–10% of the embryos being affected. Interestingly, Iso induced an approximately 3-fold increase in the number of homozygous mutant embryos developing cardiac arrhythmia, an effect that was not observed in WT embryos (Figure 6L). Since a majority of mutants developed into adulthood, we asked whether adult *popdc1*^{s191f} mutants also displayed any pathology. To this end, we confined our analysis to skeletal muscle and studied membrane localization of Popdc1 and Popdc2. Adult homozygous mutants and WT animals were randomly picked, and Popdc1 and Popdc2 expression were assessed immunohistochemically in the trunk musculature. Similar to what we observed in patients' biopsies, membrane localization of Popdc1 and Popdc2 was significantly diminished in the mutant muscle (Figure 7, A–D). In addition, many mutant fibers displayed an increase in number and signal intensity of immunostained intracellular vesicles, particularly in the case of Popdc1 (Figure 7A), suggesting that the serine 191 to phenylalanine mutation in zebrafish resulted in impaired membrane trafficking of the mutant Popdc1 protein and Popdc2. Therefore, the phenotypic spectrum of the homozygous *popdc1*^{S191F} mutant was reminiscent of the phenotypes observed in our patients, fully supporting the notion that the *POPDC1*^{S201F} mutation is pathogenic and causes heart and muscle disease.

Discussion

Our work demonstrates that mutations in *POPDC1* are responsible for heart and muscle pathologies. Indeed, WES identified the disease-segregating homozygous missense mutation S201F in *POPDC1* in a family with LGMD and AV block. Further screening of *POPDC1* mutations in 104 patients with heart and/or myopathic phenotypes resulted in a negative outcome for the presence of homozygous or compound heterozygous mutations, as expected for a very rare, family-specific recessive allele.

Evidence for the pathogenic nature of the *POPDC1*^{S201F} mutation was in particular obtained by the knockin mutation in zebrafish, which displayed several heart and muscle pathologies that were reminiscent of the symptoms found in the patients. Furthermore, the in vitro assays provided strong evidence for an essential role of cAMP binding to execute POPDC1's biological functions. cAMP-affinity precipitation and FRET analysis revealed that the switch from serine to phenylalanine caused an approximately 50% reduction in cAMP binding. Further evidence for reduced cAMP sensitivity and the resulting electrophysiological consequences was obtained from experiments in *Xenopus* oocytes and HL-1 cells. The fact that Iso stimulation caused an increase in the number of zebrafish mutants displaying cardiac arrhythmia suggests that the cAMP-binding ability of POPDC1 has an important physiological function

in the heart. The sarcolemmal localization of the mutant protein was reduced in the patients' muscle biopsies and in the trunk musculature of the zebrafish mutant. These data suggest that cAMP binding of POPDC1 is somehow involved in modulating its own membrane transport. Moreover, membrane trafficking of TREK-1 was impaired in the presence of mutant POPDC1^{S201F} protein. Similarly, POPDC2 displayed a trafficking defect in muscle tissue, suggesting that cAMP binding of POPDC1 not only modulates its own membrane trafficking, but also that of associated proteins. Mutations in *POPDC1*, which cause a lack or a reduction in cAMP affinity, may actually result in a gain of function, increasing hyperpolarization and upstroke velocity of the cardiac action potential. Both parameter changes could be interpreted as effects of POPDC1 on TREK-1 current. However, it is unlikely that TREK-1 alone is sufficient to fully explain the clinical phenotypes observed in the patients. Nonetheless, this protein-protein interaction served throughout our study as a surrogate to assess POPDC protein family function. Further work will be required to identify additional POPDC interaction partners; this may provide additional opportunities to better define the molecular basis for the observed cardiac arrhythmia phenotype.

Markedly, impaired membrane trafficking was reported in many forms of muscular dystrophy, especially those caused by mutations in CAV3, DYS, and DYSF (27). However, no discernible effects on the plasma membrane levels of these proteins were observed in our patients, despite the fact that each of them was coimmunoprecipitated with POPDC1. The effects of POPDC1 on CAV3, DYS, and DYSF may be subtle and not discernible by immunohistochemistry. We may speculate that these interactions might be more important in response to plasma membrane rupture or during muscle regeneration (13). Therefore, the physiological and pathophysiological roles for these protein-protein interactions have yet to be defined.

The *Xenopus* oocyte experiments demonstrated a dual impact of POPDC1 on TREK-1, with both processes being modulated by cAMP. We observed a cAMP-dependent increase in membrane localization of TREK-1 as well as a decrease in channel gating. We recently proposed 2 alternative models to describe how POPDC1 might modulate ion channel function: the switch and the cargo model (9). The cargo model proposes that POPDC1 might be involved in membrane trafficking. Our data give further support to this model, since cAMP binding to POPDC1 causes an increase in membrane localization. It is noteworthy that an interaction of POPDC1 with the vesicle-associated membrane protein VAMP3 has recently been reported (28). However, the significance of this interaction with regard to the regulation of membrane localization in skeletal muscle is presently unclear and deserves further study.

The switch model predicts that cAMP binding induces a conformational change in the POPDC1 protein, affecting the biological properties of interacting proteins. Ligand-induced conformational changes have been described for other cAMP effector proteins (29), and the POPDC1/TREK-1 FRET data suggest a similar structural remodeling in the case of POPDC1 However, the switch model is not supported by the fact that the TREK-1 current in oocytes is not acutely affected by cAMP, suggesting a more complex regulation. Furthermore, in the presence of S201F, membrane transport of TREK-1 is impaired; however, an increase in current can be measured. These paradoxical results could be explained by the fact that cAMP not only binds POPDC1, but also activates other effector proteins. For example, it is well established that protein kinase A interferes with TREK-1 gating through phosphorylation (30, 31). Our unpublished mapping data place the POPDC1-binding site in the vicinity of the PKA-dependent phosphorylation site of TREK-1. It is therefore possible that binding of POPDC1 to TREK-1 results in steric interference with PKA-dependent phosphorylation, thereby indirectly shielding TREK-1 from PKA-mediated inactivation. Experiments with a TREK-1 mutant, which lacks the PKA-dependent phosphorylation site, or pharmacological studies using PKA inhibitors will be informative in this context (32). Interestingly, POPDC1 is also subject to β-adrenergic–dependent phosphorylation (33, 34). Thus, the regulation of POPDC1 involving cAMP binding, subcellular localization, and phosphorylation of itself and of interacting proteins deserves further investigations.

POPDC1^{S201F} causes a mild, late-onset LGMD. The pathogenesis of the muscle damage is supported by the muscular dystrophy phenotype that we observed in a significant fraction of homozygous *popdc1^{S191F}* zebrafish mutants. Detachment of muscle fibers from the MTJ was evident, as reported in many other zebrafish mutants with dystrophic phenotypes (25, 26, 35–37). The myofiber detachment is probably based on the failure of proper ECM formation, as demonstrated by TEM. It can be envisioned that the lack of proper matrix assembly provides insufficient mechanical linkage, leading to fiber detachment when the zebrafish larvae start to swim. Identical phenotypes were observed for *popdc1* (this study and Supplemental Figure 14) and *popdc2* morphants (15), suggesting that both genes are probably acting together in the same pathway. Presently, it is unclear how POPDC proteins are linked to MTJ formation and ECM accumulation and what role cAMP signaling might have in these processes; however, the fact that POPDC1 interacts with DYS (and DYSF and CAV-3) suggests that it might be involved in laminin-DAG linkage formation (37, 38). In skeletal muscle, laminins connect the muscle cell to the ECM by binding either dystroglycan or integrins at the cell membrane. Epistasis experiments will be required to find out whether POPDC1 is interacting with dystroglycan (possibly via DYS), integrins, or both. Alternatively, POPDC1 may be involved in matrix deposition, as POPDC1 has recently been implicated in autocrine matrix deposition (39).

In conclusion, we have discovered a disease gene, *POPDC1*, causing a very rare LGMD with recessive inheritance and mild disease progression in skeletal muscle. However, the heart is strongly affected by this mutation, producing a severe form of AV block. Aberrant membrane trafficking and ECM abnormalities probably form the molecular basis for the observed heart and skeletal muscle phenotypes present in this family. The functional interaction of POPDC1 with a variety of membrane and membrane-associated proteins opens up perspectives for studying the genetic basis of cardiac and skeletal muscle disease and other phenotypes that are related to the main or corollary functions of *POPDC1*.

Methods

WES. Exome sequencing was performed using genomic DNA of the 2 affected brothers (PTIII-1 and PTIII-2) and both parents using NimbleGen Sequence Capture technology (SeqCap EZ Human Exome Library v2.0) according to the manufacturer's instructions. The enriched librar-

ies underwent 90 base pair, paired-end sequencing on a HiSeq2000 next-generation sequencing platform (Illumina) at an average of 80× coverage. SOAPaligner (soap2.21) was used to align clean reads to the human reference genome (UCSC hg19, build 37.1), and SNP calling used the SOAPsnp (v.1.03), while BWA and the Genome Analysis Tool Kit (GATK) were used for the detection of indels. After filtering PCR duplicates, some public databases, including dbSNP135 (with frequency greater than 0.5%), 1000 Genome variants database, HapMap exomes, and an in-house database, which contains WES data from approximately 1,000 normal individuals, were used to filter out previously reported variants. As disease-causing variants have a very high probability of causing amino acid changes, we initially focused on nonsynonymous variants and splice-site and indel mutations. For potential disease-causing variants, the consequences of the amino acid changes were predicted using Polyphen2 (40), SIFT (41), and Pmut (42). In order to confirm that the variation was not the product of sequencing errors, PCR amplification and Sanger sequencing were performed on the variant. Primer pairs to amplify the sequence surrounding the mutation were synthesized (POPDC1 Exon 4–forward, AAATACTTGTGCCTCAAGAAGTGC; POPDC1 Exon 4–reverse, CCCCCAATAATTCATAGCAGTG), and the PCR was run in a final volume of 25 μl containing 100 ng genomic DNA, 20 mM Tris–HCl (pH 8.4), 50 mM KCl, 1.5 mM MgCl2, 0.2 mM dNTPs, 5 U Taq DNA Polymerase (Invitrogen), and 0.4 μl of each primer. The amplified PCR product was analyzed by direct sequencing on an automatic sequencer (ABIPRISM 3130, Applied Biosystems). DNA library construction and target capture were performed following the manufacturer's protocol before sequencing on the SOLiD 5500xl (Life Technologies) using a paired-end protocol (read length 75 bp + 35 bp). Reads were demultiplexed and aligned to a human reference genome (hg19). Duplicate reads and those with low mapping quality score (<8) were removed. Variant calling was carried out using diBayes (SNPs) and small indel modules as well as GATK v1.5-20 and Samtools v0.1.18. Alignment and coverage metrics were calculated using Picard v1.40, BedTools v2.12, and in-house Perl scripts. GATK CallableLoci Walker was used to identify target genomic regions covered sufficiently for variant calling (minimum depth > 4 with base quality > 20 and mapping quality > 10).

POPDC1 mutation screening in patients. We screened an additional 104 unrelated patients with different clinical features, including cardiac arrhythmia, AV block, sudden death, and LGMD (see Supplemental Table 1), for mutations in *POPDC1*. Genomic DNA from patients was extracted from peripheral lymphocytes by standard methods. PCR primers (Supplemental Table 2) were designed to amplify all 7 exons of *POPDC1* as well as their flanking intronic regions. PCRs were run and analyzed under the conditions described above.

Immunohistochemistry. The 10-μm frozen sections of skeletal muscle biopsies of patients PTI-1 and PTIII-2 and 2 control biopsies or muscles dissected out from adult WT and *popdc1*$^{S191F/S191F}$ zebrafish were mounted on Superfrost Plus glass slides (Thermo Fisher Scientific) and subjected to immunohistochemistry using the following primary antibodies: POPDC1 (HPA018176, Sigma-Aldrich), POPDC2 (HPA024255, Sigma-Aldrich), DYS (D8043, Sigma-Aldrich), CAV3 (610420, BD Transduction Laboratories), DYSF (NCL-Hamlet, Leica), α-sarcoglycan (NCL–α-SARC, Leica), and dystroglycan (MANDAG2[7D11], DSHB). For the detection of primary antibodies, the following secondary antibodies were employed: Alexa Fluor 488–conjugated donkey anti-rabbit (A-21206, Invitrogen) and Alexa Fluor 555–conjugated donkey anti-mouse (A31570, Invitrogen). For counterstaining, DAPI (Calbiochem) was employed. The fluorescent signal was analyzed by confocal microscopy. Membrane signal intensities of approximately 30 muscle fibers were measured using Icy software and corrected for background. To calculate relative signal intensity levels, individual measurements from mutant fibers and control fibers were taken as a percentage of mean of control samples. Error bars are to 1 SD.

Immunocytochemistry. Cos-7 cells (87021302, Sigma-Aldrich) were transfected with constructs encoding HA-tagged POPDC1^{WT} or POPDC1^{S201F} alone or together with a TREK-1–Flag plasmid or myc-tagged mouse POPDC1 together with HA-tagged DYSF and stained 24 hours later with anti-HA (MMS-101R, Covance), anti-Flag (F1804, Sigma-Aldrich), or anti-myc (clone 9c,10, ab32 Abcam) antibodies. As secondary antibodies, FITC-conjugated anti-mouse Fab fragments (715-097-003, Jackson ImmunoResearch Laboratories) and Alexa Fluor 555–conjugated donkey anti-mouse (A31570, Invitrogen) were used. HL-1 cells (provided by Emmanuel Dupont, Imperial College London) were stained using anti-POPDC1 (HPA018176, Sigma-Aldrich) and anti-POPDC2 (HPA024255, Sigma-Aldrich) as primary and Alexa Fluor 594–conjugated donkey anti-rabbit (A-21207, Invitrogen) as secondary antibodies. Nuclei were stained with DAPI (Calbiochem). Images were taken using a Zeiss LSM 510 confocal microscope.

Live cell imaging (FRET analysis). 293A cells (R705-07, Thermo Fisher Scientific) were transfected with POPDC1^{WT}-CFP or POPDC1^{S201F}-CFP together with YFP–TREK-1 plasmids at a 5:1 ratio. Forty-eight hours later, live cell imaging was performed exactly as described previously (10).

Mutagenesis. The S201F point mutation was introduced into POPDC1 cDNA by PCR using the following primers: POPDC1-S201F$_s$, 5′-AACATTTACCCCTGTGCCTTTAT AGATTTTCCTGAATTTAGATCAAC-3′; POPDC1-S201F$_{as}$, 5′-GTTGATCTAAATTCAGGAAAATCTATAAAGGCACAGGGGTAAATGTT-3′ (mutant nucleotides are underlined). Correct mutagenesis was confirmed by sequence analysis. For injection into *Xenopus* oocytes and zebrafish eggs, cDNAs were subcloned into pSGEM. For expression in mammalian cell lines, cDNAs were subcloned into the pECFP-N1 vector (Clontech). PCR was used to generate *POPDC1* constructs that encode proteins fused at their carboxy termini to a HA epitope tag.

Tissue lysates. For determining expression levels, proteins were extracted from skeletal muscle using 50 mM Tris, pH 8.0, 4 M urea, 10% SDS, and 2 mM EDTA, pH 8.0. Protein concentrations of lysates were estimated with the help of the DC Protein Assay (Bio-Rad), and equal amounts of proteins were subjected to gel electrophoresis and Western blot analysis. To reduce protein aggregation, lysates were incubated at 37°C for 30 minutes or 60°C for 15 minutes in SDS loading buffer.

cAMP-affinity precipitation. Cos-7 cells (87021302, Sigma-Aldrich) were transfected with POPDC1^{WT} or POPDC1^{S201F} constructs with HA epitope tags attached to their C termini using Lipofectamine 2000 reagent (Invitrogen), and cells were harvested 24 hours later using a buffer containing 50 mM Tris, pH 8.0, 150 mM NaCl, 2 mM EDTA, pH 8.0, 1% (v/v) Triton X-100, 0.25% (w/v) gelatin, and protease inhibitors (Roche). Cell lysates were briefly sonicated and cleared twice by centrifugation at approximately 18,000 *g* at 4°C for 30 minutes. Then 30 μl of the lysates were taken as loading controls. Lysates were first incubated with 50 μl ethanolamine (EtOH-NH) agarose (BioLog) for 1 hour with rotation at 4°C. After centrifugation at 500 *g* at 4°C for 5 minutes, the supernatant was supplemented with 1 mM IBMX (3-isobutyl-1-methylxanthine; Sigma-Aldrich) and

added to 4.8 mg cAMP agarose (A0144, Sigma-Aldrich). After incubation for 2 hours with rotation at 4°C, both EtOH-NH and cAMP agaroses were washed with wash buffer A (10 mM HEPES, pH 7.4, 1.5 mM $MgCl_2$, 10 mM KCl, 500 mM NaCl, 0.1% [v/v], Igepal CA-630, 1 mM DTT, 1 mM IBMX) followed by 3 washes with wash buffer B (10 mM HEPES, pH 7.4, 1.5 mM $MgCl_2$, 10 mM KCl, 0.1% [v/v], Igepal CA-630, 1 mM DTT). Agarose-bound proteins were eluted in SDS sample buffer by boiling at 96°C for 5 minutes and subjected to gel electrophoresis and Western blot.

Gel electrophoresis and Western blot. Proteins were size separated and transferred onto nitrocellulose membrane (BioTrace NT, Pall). The membrane was washed with TBST (50 mM Tris-HCl, pH 7.4, 150 mM NaCl, 0.1% [v/v] Tween-20) and blocked in 5% (w/v) low-fat milk in TBST for 1 hour at room temperature and subsequently incubated with anti-HA (MMS-101R, Covance), anti-FLAG (F1804, Sigma-Aldrich), anti-actin (sc-1616, Santa Cruz Biotechnology Inc.), anti-POPDC1 (sc-49889, Santa Cruz Biotechnology Inc.), or anti-POPDC2 (HPA024255, Sigma-Aldrich) overnight at 4°C. For peptide competition assays, membranes were incubated with POPDC1 or POPDC2 antibodies together with a 10-fold excess of the respective neutralizing peptide (sc-49889 P [POPDC1], Santa Cruz Biotechnology Inc., APrEST72859 [POPDC2], Atlas Antibodies). After several washes, the blots were incubated for 1 hour at room temperature with horseradish peroxidase–coupled anti-mouse (PI-2000, Vector Laboratories), anti-goat (PI-9500, Vector Laboratories), or anti-rabbit antibodies (PI-1000, Vector Laboratories). After washing, signals were detected using an enhanced chemiluminescence protein detection method (Millipore). Exposed films were digitalized and band intensities were determined using ImageJ (43). Ratios between input and cAMP agarose–bound protein fractions were calculated and values were statistically analyzed using GraphPad Prism.

Coimmunoprecipitation analysis. For coimmunoprecipitation (Co-IP) analysis, Cos-7 cells (87021302, Sigma-Aldrich) were transiently transfected with myc-tagged Popdc1 and either Becker DYS, M2-microdystrophin (provided by Rolf Stucka, Ludwig-Maximilans-Universität, Munich, Germany), FLAG-tagged Dp71 DYS (GenScript), or DYSF-3HA provided to Addgene (plasmid catalog 29767) by Steven Vogel (NIH, Bethesda, Maryland, USA) (44); empty vectors were transfected as negative controls. Protein lysates were produced as described above. A sample was taken as input control, and the rest of the lysates were subjected to Co-IP using the ProFound c-Myc Tag IP/co-IP Kit (23620, Thermo Fisher Scientific) or the Pierce HA Tag IP/Co-IP Kit (26180, Thermo Fisher Scientific) following the manufacturer's instructions.

Zebrafish strains and lines. Zebrafish AB and *popdc1*^{S191F} lines were maintained under standard conditions at 28.5°C according to established protocols (45). Zebrafish were raised and staged in hours post fertilization (hpf) or dpf. Pigmentation was inhibited with 0.2 mM 1-phenyl-2-thiourea (PTU) in egg water.

Morpholino design and microinjections. Morpholino-modified oligonucleotides (MO) were obtained from Gene Tools LLC. Embryos were injected at the 1- to 2-cell stage with 0.5 ng to 2 ng of *popdc1*-specific morpholino; coinjection of *p53*-targeting morpholino (5′-GCGCCATTGCTTTGCAAGAATTG-3′) was performed to suppress nonspecific morpholino toxicity. Morpholinos targeting *popdc1* were directed against the splice-acceptor site of exon 4 (MO1-*popdc1*, 5′-CTTAATCTGGAATTAAACAGGAGAA-3′) and the splice donor site of exon 4 (MO2-*popdc1*, 5′-TACTTTCCTTTGAGAAGAATGCTGA-3′).

Gene editing. A *popdc1*^{S191F} mutation was generated using the GoldyTALEN modified scaffold (46). The left TALEN (P1E5_S191FL: 5′-AACATTTTACACCAATGCCTT-3′) and right TALEN (P1E5_S191FL: 5′-CATCTGAGTTGACCTGAA-3′) were assembled via the GoldenGate method. For ease of analysis, TALEN recognition sequences flanked a *Ple*I restriction site in exon 5 of *popdc1*, which was destroyed upon successful targeting. TALEN repeat variable di-residues (RVDs) were cloned into a pT3TS-driven TALEN scaffold. Resulting mRNA was injected into 1-cell–stage zebrafish embryos. For S191F mutagenesis, the following oligonucleotide was coinjected together with the TALEN constructs: S191F oligonucleotide, CACCAATGCCT**TC**ATCGACTTCCCAGAATTCAGGTCAA (underlined triplet encodes F191; bold letters indicate which nucleotides were mutated). Larvae were molecularly tested at 2 dpf or raised for germline mutation analysis. Somatic and germline TALEN-induced mutations were evaluated by PCR and restriction fragment length polymorphisms. The primer pair P1TALE5_1434F, 5′-TCAGAAATCCAGACAGCCGTG-3′ and P1TALE5_2175R, 5′-AGTTCTCCTCAGCAGCGATC-3′ was used to amplify the locus. Subsequently, the PCR fragment was restriction digested with *Ple*I. The mutant allele produced a 741-bp fragment, while the WT allele produced 2 fragments of 365 and 375 bp. For further analysis, the PCR products were sequenced with the following primer sequences: P1TALE5_1556F, 5′-CAAAACAATAATGGCAGACTG-3′ and P1TALE5_2069R, 5′-TCTTTTTTATTTGTGTGTAGGGAA-3′. Heterozygotes were backcrossed 6 times with the AB line in order to outcross any off-target mutations. Homozygous mutant and WT animals were bred separately.

Forced expression. The human POPDC1^{WT} and POPDC1^{S201F} cDNAs were subcloned into the psGEM vector. To generate mRNA, the clones were linearized with *Xho*I and capped mRNA was synthesized using the T7 mMessage Machine Kit (Ambion).

Whole-mount in situ hybridization. Whole-mount in situ hybridization was carried out as described previously (15). A partial clone of *popdc1* cDNA was subcloned into the pGEMTeasy vector (Promega). A digoxygenin-labeled antisense probe was generated using T3 polymerase after linearization with *Bam*HI.

Whole-mount immunohistochemistry and rhodamine-phalloidin staining. Whole-mount immunostaining was performed as described previously (15). The following primary antibodies were used: monoclonal F59 (DHSB), monoclonal F310 (DHSB), monoclonal anti-sarcomeric α-actinin (A7811, Sigma-Aldrich), anti-DYS (D8043, Sigma-Aldrich), and anti-vinculin (FAK100, Millipore). Alexa Fluor 488–coupled donkey anti-mouse (A21202, Invitrogen) was used as secondary antibody. For F-actin staining, zebrafish embryos were incubated with rhodamine-phalloidin (R415, Invitrogen). Stained zebrafish embryos were embedded in 1% low melting agarose and imaged by confocal microscopy (Zeiss, LSM 510).

Live in vivo cardiac imaging. The heart rate of zebrafish morphants was recorded using a Leica imaging system equipped with a VGA Miniature GigE CCD Color Camera (DFK 23G618, Scorpion Vision). Video images were recorded at 28°C and processed with ImageJ (43) to obtain heart rate measurements and perform M-mode analysis. For in detail analysis of the arrhythmic phenotype, cardiac performance batches were screened for individuals showing arrhythmic phenotypes without cardiac edema. Cardiac contractility was recorded in tricaine-anesthetized 6- to 9-dpf embryos. For pharmacological characterization of the phenotype, 50 homozygous Popdc2^{S181F} individuals were incubated in

10^{-4} M Iso (experimental group) or water (control) for 5 minutes. The percentage of animals displaying cardiac arrhythmia was determined. The imaging system consisted of a custom-made selective plane illumination microscope (SPIM) equipped with an Olympus UMPLFLN 20 × W objective and a digital high-speed video camera, Hamamatsu Orca Flash 4.0, in transmitted light mode. Images were recorded at 28°C (2,000 images, 100 fps) and imported into Fiji (47). Luminance periodograms of pixels being passed by the ventricle or atrium were filtered by an equi-ripple low-pass filter with a pass frequency of 0.1 Hz and a stop frequency of 10 Hz (Lab View 2013, National Instruments). In these filtered periodograms, peaks were detected and peak-to-peak distances (reflecting beat-to-beat distances) were converted to a beat-to-beat frequency for each interval. These frequencies were plotted against time to a cardiotachiogram to calculate mean heart rate. Stroke volume was determined as described (48).

TEM. Five-dpf WT or *popdc1*$^{S191F/S191F}$ zebrafish larvae were sacrificed using MS-222 and fixed in 2.5% (v/v) glutaraldehyde in 0.1 M sodium cacodylate buffer (pH 7.4) at 4°C overnight and then postfixed in 1% (w/v) osmium tetroxide in 0.1 M sodium cacodylate buffer at room temperature for 1 hour. After 2 buffer washes, samples were dehydrated using a graded ethanol series of 50%, 70%, 90%, and 100% (v/v). Larvae were then immersed in propylene oxide and infiltrated with 1:1 propylene oxide/araldite resin (Agar Scientific) overnight and then in pure resin for 2 hours. After several changes of resin, samples were embedded and the resin was polymerized at 60°C for 24 hours. After polymerization, 100-nm–thick sections were cut with an ultramicrotome and mounted on 300 mesh copper TEM grids. Thereafter, samples were poststained using uranyl acetate and TEM was performed with a JEOL 1200 EX electron microscope.

Measurement of TREK-1 current. *Xenopus laevis* was maintained and oocytes isolated under standard conditions according to established protocols. Capped cRNA transcripts were synthesized in vitro using the mMessage mMachine T7 transcription kit (Ambion). The cRNAs were purified and photometrically quantified. Human TREK-1c alone or together with human POPDC1 (WT or S201F mutant) was injected into *Xenopus laevis* oocytes at the indicated amounts of cRNA. Oocytes were incubated at 19°C for 24 to 48 hours in ND96 solution containing 96 mM NaCl, 2 mM KCl, 1 mM $MgCl_2$, 1.8 mM $CaCl_2$, and 5 mM HEPES (pH 7.4–7.5) supplemented with 50 mg/l gentamicin and 275 mg/l sodium pyruvate. For experiments with elevated cAMP levels, 25 mM theophylline or 1 mM 8-Br-cAMP (Tocris Bioscience) was supplemented to the storage solution, directly following the cRNA injection. Two-microelectrode voltage-clamp measurements were performed with a Turbo Tec-10 C amplifier (npi, Tamm). Data were recorded at a sampling rate of 2 kHz and lowpass filtered with 700 Hz. The oocytes were placed in a small-volume perfusion chamber and superfused with ND96 solution. Oocytes were held at –80 mV, and voltage was ramped from –120 to +45 mV within 3.5 seconds using a sweep time interval of 4 seconds. Since current amplitudes varied from 1 batch of oocytes to the next, currents were normalized to TREK-1c WT current amplitudes of the respective batch and recording day.

Patch-clamp experiments of HL-1 cells. HL-1 cells, provided by William C. Claycomb (Louisiana State University, Baton Rouge, Louisiana, USA) (22), were transfected as described above. Action potentials were recorded in the whole-cell configuration under current clamp conditions at room temperature (22°C). For patch-clamp experiments, HL-1 cells were superfused with solution containing 135 mM NaCl, 5 mM KCl, 1 mM $CaCl_2$, 1 mM $MgCl_2$, 0.33 mM NaH_2PO_4, 10 mM glucose, 2 mM sodium pyruvate, and 5 mM HEPES (pH 7.4 with NaOH) as previously described (49, 50). Patch-clamp experiments were performed in the whole-cell configuration using pipettes pulled from borosilicate glass capillaries. The pipettes had a tip resistance of 3.0 to 4.0 MΩ when filled with a solution containing 60 mM KCl, 65 K^+-glutamate, 5 mM EGTA, 2 mM $MgCl_2$, 3 mM K_2ATP, 0.2 mM Na_2GTP, and 5 mM HEPES (pH 7.2 with KOH). Data acquisition and command potentials were controlled with a commercial software program (Patchmaster, HEKA) with a sweep time interval of 1 second and a sample rate of 200 kHz. Data analysis of action potentials was done using Fitmaster software (HEKA). For each cell measured, the action potential parameters were averaged by analyzing 10 subsequent action potentials, as previously described (49).

RT-PCR. Total RNA was isolated from HL-1 cells using High Pure RNA Isolation Kit (Roche) containing DNAseI. Reverse transcription (RT) was performed with Superscript II reverse transcriptase (Invitrogen) according to the manufacturer's instructions. PCR was performed using Taq Gold Polymerase (Applied Biosystems) according to the manufacturer's instructions. Reaction mixtures were preheated at 96°C for 5 minutes, followed by 40 cycles at 96°C for 30 seconds, 58°C for 30 seconds, and 72°C for 45 seconds. PCR products were visualized by gel electrophoresis on 2% agarose gels. The following intron-spanning primers were used: GAPDH forward, 5′-ACTTCAACAGCAACTCCCACTCT-3′, GAPDH reverse, 5′-GCTGTAGCCGTATTCATTGTCATA-3′; TREK-1 forward, 5′-G ACGAACTCATCCAGCAAATAGTG-3′, TREK-1 reverse, 5′-AAAGAAGAAAGAGCTTCCGAGGTC-3′. For both primer pairs, the amplification products were confirmed by sequencing. RNA that was not reverse transcribed was used as negative control.

Statistics. Results are presented as mean ± SEM. Statistical significance was defined as $P < 0.05$.

Study approval. Informed consent for WES analysis and clinical exome analysis for the family was obtained. Approval of the Ethical Committee University Hospital Ferrara was given to the project as follows: Neuromics, approved May 30, 2013, approval number 05/2013, P. 58-2013; RARER, approved June 20, 2013, approval number 06/2013, P. 95-2013 and routine molecular diagnosis approval number 26/7/2012, P. 7/2012. The zebrafish work at Imperial College London was approved by the Animal Welfare and Ethical Review Board of the Harefield Heart Science Centre and licensed by the United Kingdom Home Office (PPL 70/7171). The zebrafish work at the University of Innsbruck was approved by the Austrian Bundesministerium für Bildung, Wissenschaft, und Kultur (animal ethics permission GZ 66.008/0004-II/3b/2012). The work with *Xenopus* at the University of Marburg was approved by the Regierungspräsidium Gießen, Germany (V54-19c 20 15 hours 02 MR 20/28 Nr.A 4/2013).

Author contributions

RFRS, BOB, SS, TS, KLP, SR, A Froese, VON, CG, TM, GT, and PS designed and conducted functional experiments. FD, FF, BD, and EB clinically characterized the family. AP clinically supervised the project on the families of 4 (RARER). CR and EA clinically characterized the patients with cardiac abnormalities screened for mutations. CS, CP, FRDR, RS, FG, MN, WL, HJ, and XX performed the DNA studies, patient screening, and technical validation. JZ and MF performed the WES and bioinformatics analysis. JW designed WES studies. ND designed and analyzed the electrophysiological

studies and helped write the manuscript. TB and A Ferlini designed research studies, analyzed data, and wrote the manuscript.

Acknowledgments

This research was financed by BIO-NMD (EU FP7 grant n. 241677 to A. Ferlini) and RARER (grant 1A Regione Emilia Romagna n.6/7/2012, to A. Pietrangelo and A. Ferlini), the Medical Research Council (MR/J010383/1), the British Heart Foundation (PG/14/46/30911, PG/14/83/31128), and the Magdi Yacoub Institute (to T. Brand) and was also supported by NEUROMICS (EU FP7 n.305121), the Deutsche Forschungsgemeinschaft (DE-1482/3-1) (to N. Decher), the Anneliese Pohl-Stiftung, the Universitätsklinikum Gießen und Marburg (to S. Rinné), and the Gertraud and Heinz Rose Foundation (to V.O. Nikolaev). The monoclonal antibody β-dystroglycan (MANDAG2[7D11]) was developed by Glenn E. Morris (Wolfson Centre for Inherited Neuromuscular Disease, Oswestry, United Kingdom). F59 and F310 were developed by Frank E. Stockdale (Stanford University, Stanford, California, USA) and obtained from the Developmental Studies Hybridoma Bank, created by the Eunice Kennedy Shriver National Institute of Child Health and Human Development (NICHD) of the NIH and maintained at The University of Iowa, Department of Biology, Iowa City, Iowa, USA. We thank Jan Huisken and Michael Weber (Max-Planck-Institute of Molecular Cell Biology and Genetics, Dresden, Germany) for their valuable help in setting up the SPIM microscope in the lab of T. Schwerte. We thank Ursula Herbort-Brand (Imperial College London) for excellent technical assistance.

Address correspondence to: Jun Wang, BGI-Shenzhen, Building No. 11, Beishan Industrial Zone, Yantian District, Shenzhen 518083, China. Phone: 86.0755.250199; E-mail: wangj@genomics.cn. Or to: Thomas Brand, Harefield Heart Science Centre, National Heart and Lung Institute, Imperial College London, Hill End Road, Harefield, UB96JH, United Kingdom. Phone: 44.1895.45.3826; E-mail: t.brand@imperial.ac.uk. Or to: Alessandra Ferlini, Unit of Medical Genetics, Department of Medical Sciences, University of Ferrara, Via Fossato di Mortara, 74, 44121 Ferrara, Italy. Phone: 39.0532.974439; E-mail: fla@unife.it.

Kar-Lai Poon's present address is: Institute of Molecular and Cell Biology, Singapore.

Viacheslav Nikolaev's present address is: Institute of Experimental Cardiovascular Research, Hamburg, Germany.

1. Allen HD, Thrush PT, Hoffman TM, Flanigan KM, Mendell JR. Cardiac management in neuromuscular diseases. *Phys Med Rehabil Clin N Am*. 2012;23(4):855–868.
2. Hermans MC, Pinto YM, Merkies IS, de Die-Smulders CE, Crijns HJ, Faber CG. Hereditary muscular dystrophies and the heart. *Neuromuscul Disord*. 2010;20(8):479–492.
3. Wicklund MP, Kissel JT. The limb-girdle muscular dystrophies. *Neurol Clin*. 2014;32(3):729–749.
4. Groh WJ. Arrhythmias in the muscular dystrophies. *Heart Rhythm*. 2012;9(11):1890–1895.
5. Kostareva A, Sejersen T, Sjoberg G. Genetic spectrum of cardiomyopathies with neuromuscular phenotype. *Front Biosci (Schol Ed)*. 2013;5:325–340.
6. Puckelwartz M, McNally EM. Emery-Dreifuss muscular dystrophy. *Handb Clin Neurol*. 2011;101:155–166.
7. Nigro V, Savarese M. Genetic basis of limb-girdle muscular dystrophies: the 2014 update. *Acta Myol*. 2014;33(1):1–12.
8. Andree B, et al. Isolation and characterization of the novel popeye gene family expressed in skeletal muscle and heart. *Dev Biol*. 2000;223(2):371–382.
9. Brand T, Simrick SL, Poon KL, Schindler RF. The cAMP-binding Popdc proteins have a redundant function in the heart. *Biochem Soc Trans*. 2014;42(2):295–301.
10. Froese A, et al. Popeye domain containing proteins are essential for stress-mediated modulation of cardiac pacemaking in mice. *J Clin Invest*. 2012;122(3):1119–1130.
11. Korfali N, et al. The nuclear envelope proteome differs notably between tissues. *Nucleus*. 2012;3(6):552–564.
12. Alcalay Y, et al. Popeye domain containing 1 (Popdc1/Bves) is a caveolae-associated protein involved in ischemia tolerance. *PLoS One*. 2013;8(9):e71100.
13. Andrée B, Fleige A, Arnold HH, Brand T. Mouse Pop1 is required for muscle regeneration in adult skeletal muscle. *Mol Cell Biol*. 2002;22(5):1504–1512.
14. Simrick S, Schindler RF, Poon KL, Brand T. Popeye domain-containing proteins and stress-mediated modulation of cardiac pacemaking. *Trends Cardiovasc Med*. 2013;23(7):257–263.
15. Kirchmaier BC, et al. The Popeye domain containing 2 (popdc2) gene in zebrafish is required for heart and skeletal muscle development. *Dev Biol*. 2012;363(2):438–450.
16. NCBI. dbSNP - Short Genetic Variations. NIH Web site. http://www.ncbi.nlm.nih.gov/SNP/. Updated May 21, 2014. Accessed November 9, 2015.
17. 1000 Genomes - A Deep Catalog of Human Genetic Variation. 1000 Genomes Web site. http://browser.1000genomes.org/index.html/. Updated October 16, 2014. Accessed November 9, 2015.
18. NHLBI Exome Sequencing Project. Exome Variant Server. Washington University Web site. http://evs.gs.washington.edu/EVS/. Updated May 14, 2015. Accessed November 9, 2015.
19. Exome Aggregation Consortium. ExAC Database. Broad Institute Web site. http://exac.broadinstitute.org. Updated May 14, 2015. Accessed November 9, 2015.
20. Bansal D, et al. Defective membrane repair in dysferlin-deficient muscular dystrophy. *Nature*. 2003;423(6936):168–172.
21. Magri F, et al. Frequency and characterisation of anoctamin 5 mutations in a cohort of Italian limb-girdle muscular dystrophy patients. *Neuromuscul Disord*. 2012;22(11):934–943.
22. Claycomb WC, et al. HL-1 cells: a cardiac muscle cell line that contracts and retains phenotypic characteristics of the adult cardiomyocyte. *Proc Natl Acad Sci U S A*. 1998;95(6):2979–2984.
23. Yang Z, Murray KT. Ionic mechanisms of pacemaker activity in spontaneously contracting atrial HL-1 cells. *J Cardiovasc Pharmacol*. 2011;57(1):28–36.
24. Strege P, et al. Ranolazine inhibits shear sensitivity of endogenous Na^+ current and spontaneous action potentials in HL-1 cells. *Channels (Austin)*. 2012;6(6):457–462.
25. Subramanian A, Schilling TF. Thrombospondin-4 controls matrix assembly during development and repair of myotendinous junctions. *Elife*. 2014;3:e02372.
26. Bassett DI, Bryson-Richardson RJ, Daggett DF, Gautier P, Keenan DG, Currie PD. Dystrophin is required for the formation of stable muscle attachments in the zebrafish embryo. *Development*. 2003;130(23):5851–5860.
27. Posey AD Jr, Demonbreun A, McNally EM. Ferlin proteins in myoblast fusion and muscle growth. *Curr Top Dev Biol*. 2011;96:203–230.
28. Hager HA, Roberts RJ, Cross EE, Proux-Gillardeaux V, Bader DM. Identification of a novel Bves function: regulation of vesicular transport. *EMBO J*. 2010;29(3):532–545.
29. Rehmann H, Wittinghofer A, Bos JL. Capturing cyclic nucleotides in action: snapshots from crystallographic studies. *Nat Rev Mol Cell Biol*. 2007;8(1):63–73.
30. Terrenoire C, Lauritzen I, Lesage F, Romey G, Lazdunski M. A TREK-1-like potassium channel in atrial cells inhibited by β-adrenergic stimulation and activated by volatile anesthetics. *Circ Res*. 2001;89(4):336–342.
31. Patel AJ, et al. A mammalian two pore domain mechano-gated S-like K^+ channel. *EMBO J*. 1998;17(15):4283–4290.
32. Murbartián J, Lei Q, Sando JJ, Bayliss DA. Sequential phosphorylation mediates receptor- and kinase-induced inhibition of TREK-1 background potassium channels. *J Biol Chem*. 2005;280(34):30175–30184.
33. Lundby A, et al. In vivo phosphoproteomics anal-

ysis reveals the cardiac targets of β-adrenergic receptor signaling. *Sci Signal*. 2013;6(278):rs11.
34. Schechter MA, et al. Phosphoproteomic profiling of human myocardial tissues distinguishes ischemic from non-ischemic end stage heart failure. *PLoS One*. 2014;9(8):e104157.
35. Guyon JR, et al. The dystrophin associated protein complex in zebrafish. *Hum Mol Genet*. 2003;12(6):601–615.
36. Postel R, Vakeel P, Topczewski J, Knöll R, Bakkers J. Zebrafish integrin-linked kinase is required in skeletal muscles for strengthening the integrin-ECM adhesion complex. *Dev Biol*. 2008;318(1):92–101.
37. Gupta V, et al. The zebrafish dag1 mutant: a novel genetic model for dystroglycanopathies. *Hum Mol Genet*. 2011;20(9):1712–1725.
38. Kanagawa M, Toda T. The genetic and molecular basis of muscular dystrophy: roles of cell-matrix linkage in the pathogenesis. *J Hum Genet*. 2006; 51(11):915–926.
39. Benesh EC, et al. Bves and NDRG4 regulate directional epicardial cell migration through autocrine extracellular matrix deposition. *Mol Biol Cell*. 2013;24(22):3496–3510.
40. Polyphen 2. Harvard University Web site. http://genetics.bwh.harvard.edu/pph2/. Updated February 1, 2012. Accessed November 9, 2014.
41. J. Craig Venter Institute. SIFT. J. Craig Venter Institute Web site. http://sift.jcvi.org. Updated August 1, 2011. Accessed November 9, 2014.
42. PMUT. http://mmb.irbbarcelona.org/PMut/. Accessed November 24, 2015.
43. Research Services Branch. Image J. NIH Web site. http://imagej.nih.gov/. Updated October 13, 2014. Accessed November 9, 2015.
44. Covian-Nares JF1, Koushik SV, Puhl HL 3rd, Vogel SS. Membrane wounding triggers ATP release and dysferlin-mediated intercellular calcium signaling. *J Cell Sci*. 2010;123(pt 11):1884–1893.
45. Westerfield M. *The Zebrafish Book: A Guide for the Laboratory Use of Zebrafish (Brachydanio rerio)*. Eugene, Oregon, USA: University of Oregon Press; 2003.
46. Bedell VM, et al. In vivo genome editing using a high-efficiency TALEN system. *Nature*. 2012;491(7422):114–118.
47. Schindelin J, et al. Fiji: an open-source platform for biological-image analysis. *Nat Methods*. 2012;9(7):676–682.
48. Schwerte T, Fritsche R. Understanding cardiovascular physiology in zebrafish and Xenopus larvae: the use of microtechniques. *Comp Biochem Physiol A Mol Integr Physiol*. 2003;135(1):131–145.
49. Friedrich C, et al. Gain-of-function mutation in TASK-4 channels and severe cardiac conduction disorder. *EMBO Mol Med*. 2014;6(7):937–951.
50. Putzke C, et al. The acid-sensitive potassium channel TASK-1 in rat cardiac muscle. *Cardiovasc Res*. 2007;75(1):59–68.